American Mineralogist, Volume 90, pages 1402–1412, 2005

Makarochkinite, $Ca_2Fe^{2+}_4Fe^{3+}TiSi_4BeAlO_{20}$, a new beryllosilicate member of the aenigmatite-sapphirine-surinamite group from the Il'men Mountains (southern Urals), Russia

EDWARD S. GREW,[1,*] JACQUES BARBIER,[2] JIM BRITTEN,[2] MARTIN G. YATES,[1] VLADISLAV O. POLYAKOV,[3,†] ELENA P. SHCHERBAKOVA,[3] ULF HÅLENIUS,[4] AND CHARLES K. SHEARER[5]

[1]Department of Earth Sciences, University of Maine, 5790 Bryand Center, Orono, Maine 04469, U.S.A.
[2]Department of Chemistry, McMaster University, Hamilton, Ontario L8S 4M1, Canada
[3]Natural Science Museum of the Ilmen State Reserve, Miass 456317, Russia
[4]Department of Mineralogy, Swedish Museum of Natural History, Box 50007, SE-104 05 Stockholm, Sweden
[5]Institute of Meteoritics, University of New Mexico, Albuquerque, New Mexico 87131, U.S.A.

ABSTRACT

Makarochkinite, $^{[VII]}(Ca_{1.64}Na_{0.25}Mn_{0.11})^{[VI]}(Fe^{2+}_{3.56}Fe^{3+}_{1.46}Ti_{0.61}Mg_{0.25}Mn_{0.02}Nb_{0.038}Ta_{0.007})^{[IV]}(Si_{4.48}Be_{0.91}Al_{0.54}Fe_{0.07}O_{18})O_2$ (end-member $Ca_2Fe^{2+}_4Fe^{3+}TiSi_4BeAlO_{20}$) from electron-microprobe data, Mössbauer spectroscopy, and single-crystal structure refinement, occurs in a granitic pegmatite near Lake Ishkul', Il'men Mountains (Southern Urals), Il'men State Reserve, Chelyabinsk Oblast', Russia. Associated minerals include danalite, phenakite, titanite, potassian calcic amphibole (ferro-edenite and hastingsite), biotite, ilmenite, magnetite, ferrocolumbite, fergusonite-(Y), and samarskite-(Y). Makarochkinite forms equant masses 5–50 mm across, black in hand specimen; luster vitreous; it is opaque except in slivers <1 μm thick. It is brittle; Moh's hardness 5.5–6, and has no discernable cleavage; fracture is uneven. Twinning is absent. The measured density is 3.93(1) g/cm^3; calculated density 3.933 g/cm^3. It is optically biaxial, $\alpha = 1.835 \pm 0.014$ and $\gamma = 1.865 \pm 0.015$ from reflectance data, pleochroism marked: X = greenish brown, Y = yellowish brown, Z = reddish brown; $Y \leq X < Z$. Single-crystal X-ray diffraction gives triclinic symmetry, space group $P\bar{1}$, $Z = 2$, $wR(F^2)$ (all) = 0.096 for 6497 reflections, $a = 10.355(2)$, $b = 10.751(3)$, and $c = 8.873(2)$ Å, $\alpha = 105.707(8)$, $\beta = 96.227(6)$, $\gamma = 124.861(6)°$, $V = 735.7(3)$ Å^3. The eight strongest lines in the powder pattern [d-spacing (Å),(I),(hkl)] are 7.997(57)(100), 4.779(29)(011), 3.120(32)(012), 2.924(69)(0$\bar{1}$3), 2.676(77)($\bar{2}$03), 2.530(100)($\bar{2}$1$\bar{3}$), 2.410(28)(2$\bar{2}$3), 2.075(39)(4$\bar{1}$1).

Of the aenigmatite-sapphirine-surinamite group minerals, makarochkinite is compositionally closest to rhönite and høgtuvaite. It is distinguished from rhönite by $Fe^{2+} > Mg$ and by the presence of 0.91–0.98 Be per 20 cations; Be occupies the two most polymerized T sites in roughly equal amounts. Distinction from høgtuvaite is based on occupancy of the M7 site, which is dominated by Fe^{3+} in høgtuvaite and by Ti in makarochkinite.

INTRODUCTION

Four minerals of the aenigmatite-sapphirine-surinamite group (Strunz and Nickel 2001) contain essential Be: surinamite, khmaralite, welshite, and høgtuvaite (Table 1). Polyakov et al. (1986) characterized the Fe-Ti beryllosilicate "makarochkinite" as a new mineral related to aenigmatite. This relation was subsequently confirmed by single-crystal structure refinement, which gave the formula $(Ca_{1.75}Na_{0.25})(Fe^{2+}_{3.80}Fe^{3+}_{1.35}Ti_{0.60}Mg_{0.25})O_2[Si_{4.4}Al_{0.6}Be_{1.0}]O_{18}$ (Yakubovich et al. 1990), but the new mineral and name were not considered for approval by the International Mineralogical Association at that time. Grauch et al. (1994) suggested that høgtuvaite and makarochkinite are identical, whereas Hawthorne (2002) and Hawthorne and Huminicki (2002) contended that if Ti were fully ordered at a single M site as it is in aenigmatite, then makarochkinite would be the Ti-dominant analogue of høgtuvaite.

In a new crystal-structure study of makarochkinite, it was possible to independently refine the occupancy of the octahedral M7 site and confirm that Ti is the dominant cation at this site, thereby meeting the criterion of Hawthorne (2002) and Hawthorne and Huminicki (2002) for makarochkinite being distinct from høgtuvaite, whose Ti content is insufficient to be dominant at M7. The mineral and name were approved by the Commission on New Minerals and Mineral Names, International Mineralogical Association (2002-009a). The name is for Boris A. Makarochkin (1907–1988), Russian chemist and mineralogist, who studied the rare minerals from the Il'men Mountains and first collected the mineral, but described it as an amphibole (Makarochkin 1955). The original type material (sample no. 89351) is deposited in the Fersman Museum, Moscow. The neotype material (sample no. 400Shch-6) is deposited in the Natural Science Museum of the Il'men State Reserve, Miass, Russia, and in the National Museum of Natural History (Smithsonian Institution) as NMNH 174051.

* E-mail: esgrew@maine.edu
† Deceased.

0003-004X/05/0809–1402$05.00/DOI: 10.2138/am.2005.1759

Occurrence and associated minerals

Geology

Makarochkinite occurs in a pegmatite exposed in Pit 400 near Lake Ishkul' in the northern part of the Il'men Mountains (Southern Urals) within the Il'men State Reserve, city of Miass, Chelyabinsk Oblast', Russia (Fig. 1). The Il'men Mountains are underlain by the Il'meno-Vishnegorski magmato-metamorphic complex in which Lower Proterozoic metamorphic rocks are cut by a NE-trending band of nepheline syenite (miaskite) bodies with aureoles of fenite (Rasskazova 1992; Popova et al. 1996). Vein rocks associated with this band include four types of pegmatite: (1) granitic pegmatites antedating the miaskite; (2) miaskitic (nephelino-feldspathic), feldspathic, and corundum-feldspathic pegmatites giving ages of 270–290 Ma; (3) granitic pegmatites postdating the miaskite; and (4) amazonitic pegmatites giving ages of 240–260 Ma. The pegmatite exposed in Pit 400 is provisionally included in the third group.

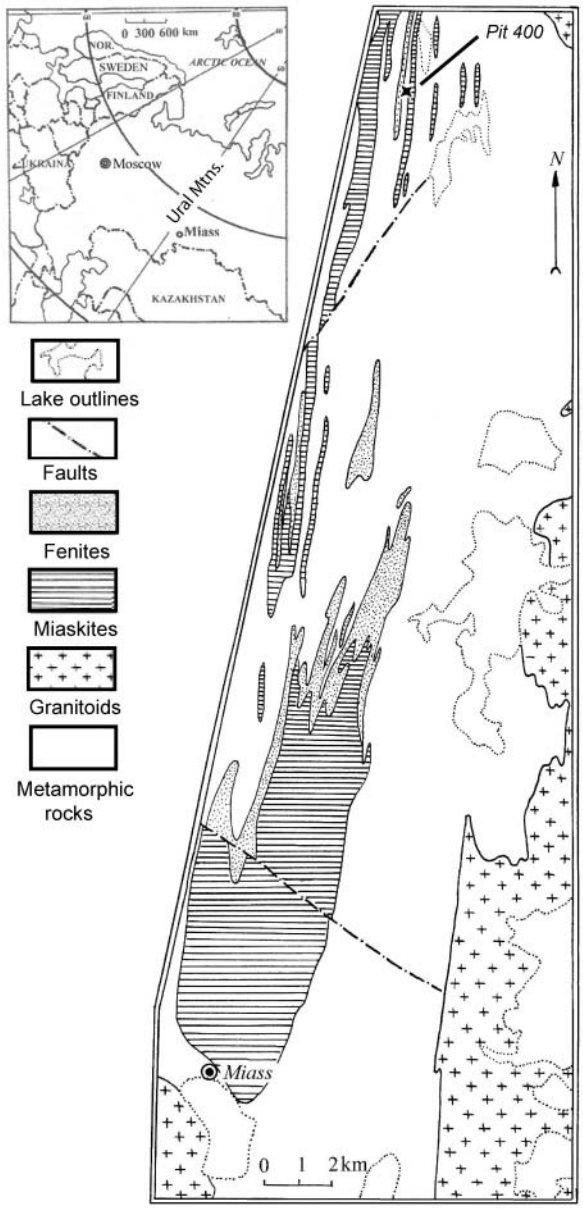

Figure 1. Geological map of the area around Miass, Russia, showing the location of Pit 400.

Makarochkin (1955, 1978) reported that Pit 400 exposed an unzoned, NS-striking vein, 0.4–0.6 m thick, of granitic pegmatite having sharp contacts with the host biotite-feldspar rocks (biotitic "syenite" and "granite gneiss"). The pegmatite body forms an elongated lens not exceeding 2 m in length and ranging from 0.2 to 0.6 m in thickness. The lens is broken into blocks by a myriad of fractures, but overall strikes 355°, i.e., roughly parallel to the banding in the host rocks. These rocks are feldspathic, biotitic, and locally amphibolitic, and become schistose and richer in biotite with abundant, disseminated titanite along the contacts with the pegmatite lens, particularly at its east contact.

Throughout much of the pegmatite body, fine- and coarse-grained pegmatite alternate in a chaotic fashion. In places, fine-grained graphic feldspar-quartz pegmatite appears to flow around detached feldspar augen up to 5 cm across; the graphic intergrowths are oriented in every direction. Segregations of accessory minerals are not associated with any particular rock type or locality within the pegmatite body. Prior to deformation, the body could have had the zonation characteristic of granite pegmatites. Zones of fine- and medium-grained graphic pegmatite are locally preserved along the contacts in the southern part of the body. A zone no thicker than 5 cm of the latter can be followed for 50–60 cm along the western contact, which is the least deformed part of the pegmatite; it is separated from the remainder of the pegmatite by a fracture coated with biotite.

Minerals

Forty two minerals have been reported from Pit 400 (Makarochkin 1955, 1978; Polyakov et al. 1986), of which 26 were identified in six specimens of host rock and pegmatite as valid species or group (Appendix 1,[1] Table 1) using optical properties, a Cameca ims 4f ion microprobe, and a Cameca SX100 electron microprobe at the University of Maine. Operating conditions for the microprobes are given in the section on makarochkinite; standards for elements requiring special attention are given in the Appendix table notes.

The host rock sample 400Shch-5 is an amphibole-biotite-titanite-plagioclase schist with accessory zircon, apatite, and ilmenite, the last mostly enclosed in titanite; the host rock in contact with pegmatite (400-21) consists of dominant oligoclase ($Ab_{82-85}An_{14-15}Or_{2-3}$), subordinate biotite (Appendix 1, Table 2), and accessory monazite, ferrocolumbite (Appendix 1, Table 3), niobian ilmenite with negligible Fe_2O_3 (Appendix 1, Table 3), hercynite ($Fe^{2+}_{0.82}Zn_{0.10}Mn_{0.05}Mg_{0.03}Al_{1.89}Fe^{3+}_{0.11}O_4$), corundum, and

[1] Deposit item AM-05-020, Appendices 1–4. Deposit items are available two ways: For a paper copy contact the Business Office of the Mineralogical Society of America (see inside front cover of recent issue) for price information. For an electronic copy visit the MSA web site at http://www.minsocam.org, go to the American Mineralogist Contents, find the table of contents for the specific volume/issue wanted, and then click on the deposit link there.

TABLE 1. Minerals of the aenigmatite-sapphirine-surinamite group containing essential Be

Mineral	End-member formula	Type locality	Environment	Source
surinamite	$Mg_3Al_3O[Si_3BeAlO_{15}]$	Bakhuis Mountains, Surinam	Metapelites and metamorphosed granite pegmatites	Baba et al. (2000); Barbier et al. (2002)
khmaralite (cf. sapphirine)	$Mg_{3.5}Al_{4.5}O_2[Si_{2.5}BeAl_{2.5}O_{18}]$	"Zircon Point", Khmara Bay, Enderby Land, Antarctica	Metamorphosed granite pegmatitic leucosomes in granulite-facies psammo-pelitic metasediments	Barbier et al. (1999); Grew et al. (2000); Christy et al. (2002)
welshite	$Ca_2(Mg_4Sb^{5+}{}_2)O_2[Si_3Be_3O_{18}]$	Långban, Sweden	Metamorphosed Fe-Mn deposit	Grew et al. (2001); Hawthorne and Huminicki (2002)
høgtuvaite	$Ca_2(Fe^{2+}{}_3Fe^{3+}{}_3)O_2[Si_4BeAlO_{18}]$	Høgtuva Window, Mo i Rana, Nordland Co., Norway	Metamorphic, in gneiss and pegmatite	Grauch et al. (1994); Burt (1994); Hawthorne (2002); Hawthorne and Huminicki (2002)
makarochkinite	$Ca_2(Fe^{2+}{}_4Fe^{3+}Ti)O_2[Si_4BeAlO_{18}]$	Ishkul' Mountain, Ilmen Natural Reserve, south Urals, Russia	Pegmatite in biotite-feldspar rocks	Polyakov et al. (1986); Hawthorne (2002); Hawthorne and Huminicki (2002)

schorl (Appendix 1, Table 2). Schorl is highly zoned: Ca varies inversely with vacancies at the X site and with Mg; Al varies inversely with Fe and (Mg + Fe).

In the pegmatite, microcline microperthite is much more dominant and coarser-grained than plagioclase. Quartz locally appears granulated and the pegmatite is foliated from cataclasis. Grain size and textural relations suggest that makarochkinite, danalite, calcic amphibole, and samarskite-(Y) are primary pegmatite minerals, as are the coarser grains of ilmenite, magnetite, and ferrocolumbite.

Beryllium minerals include a compositionally homogeneous single-crystal fragment 0.35 cm across of danalite in sample 400-21 (77% danalite, 17% helvite; 5% genthelvite; 1% Mg end-member, Appendix 1, Table 4). It is separated from plagioclase by a discontinuous, thin selvage of phenakite (Appendix 1, Table 4). In 400Shch-6, makarochkinite is locally cut by aggregates of titanite ($Ca_{1.00}Fe^{3+}_{0.05}Nb_{0.04}Al_{0.07}Ti_{0.85}Si_{1.00}O_5$), phenakite, actinolite, biotite, magnetite, K-feldspar, rare allanite-(Ce), and several Fe-rich secondary minerals, including a jarosite-like phase. These textural relations suggest that phenakite is a secondary mineral that formed from the breakdown of primary danalite and makarochkinite in these two samples.

Calcic amphibole forms masses up to 4 cm across and is olive-green in thin section. It is potassian ferro-edenite (400Shch-2) and potassian hastingsite (400-7b); stoichiometric calculations suggest significant Fe_2O_3 (Appendix 1, Table 5). Local patches of bluish color are ferrohornblende in 400Shch-2 and hastingsite in 400-7b; these patches are poorer in Ti and Na and richer in Ca than the olive-green amphibole. Biotite in flakes up to a millimeter across is titanian with little or no octahedral Al (Appendix 1, Table 2).

The relatively large grains of ilmenite (up to 2 mm) in sample 400Shch-2 contain abundant lamellae of ferrocolumbite and hematite, e.g., $(Fe^{2+}_{0.28}Mn_{0.02}Ti_{0.23}Nb_{0.03})_{\Sigma 0.56}Fe^{3+}_{1.44}O_3$. In the four samples where it was analyzed, the ilmenite is niobian, and in two, ferrian (Appendix 1, Table 3). One margin of a zoned ferrocolumbite grain in the pegmatitic portion of 400-21 is the richest in Ta of the studied samples (Appendix 1, Table 3). Magnetite contains 0.08 wt% SiO_2 (one grain), 0.2–0.4 wt% TiO_2, and 0.03–0.2 wt% Al_2O_3, V_2O_3, and MnO; Mg, Cr, Zn, Nb, Ta, and W were below detection.

A much altered Th-rich mineral in 400Shch-2 was identified as huttonite (Förster 1998) containing 74 mol% (Th,U)SiO_4, 22 mol% (REE, Y)PO_4, and 4% other (Appendix 1, Table 6). Scheelite is associated with samarskite-(Y) in 400-23.

Four Y-REE-U-Th-Nb oxides have been reported from Pit 400 (Appendix 1, Table 1). Our analyses give two distinct compositions (Appendix 1, Table 7), both of which are consistent with the formula ABO_4, where A = Ca, Mn, Fe, Y, Zr, REE, W, Th, U, and B = Ti, Nb, Ta (Hanson et al. 1999; cf. Warner and Ewing 1993, who assumed Ti to be an A-site cation). On the basis of average atomic radii for the A-site (Warner and Ewing 1993), compositions giving average radii >0.89 Å could correspond to fergusonite-(Y) and those giving average radii <0.85 Å to samarskite-(Y). However, these identifications are provisional without crystallographic studies. Minerals identified as fergusonite-(Y) include a tiny core of less altered uranian and thorian material in yellow, isotropic grains in sample 400-7b (Appendix 1, Table 7, column 3) and nearly end-member, euhedral to subequant grains mostly 20–40 μm in diameter associated with magnetite, quartz, and ferro-edenite in sample 400Shch-2 (Appendix 1, Table 7, column 2). Samarskite-(Y) forms opaque platelets 0.6–0.7 mm thick and 1.5 to over 3 mm long, rimmed by a margin of yellow, isotropic material resulting from alteration (sample 400-23). The opaque phase gives low totals, and thus could be partly hydrated as well as metamict. Our data are broadly consistent with the wet-chemical analysis for "khlopinite" reported by Makarochkin (1978) except that significant W and little Ti were found.

Geochemical environment and comparison with høgtuvaite

The makarochkinite-bearing pegmatite has many mineralogical features of the niobium-yttrium-fluorine (NYF) petrogenetic family of granitic pegmatites, more specifically, the gadolinite subtype associated with metaluminous granites (e.g., Černý 1991, 1992; Wise 1999), i.e., Y dominance in rare-earth minerals, Nb > Ta in columbite-group minerals and other oxides, and the presence of Ti and Be minerals. However, there is little evidence for F enrichment: the presence of fluorite was not confirmed in the present study, and the F contents of biotite and amphibole are relatively low.

The calcic-amphibole composition suggests that the pegmatite is not highly evolved (Claflin and Wise 2000), whereas danalite indicates low activity of alumina and moderately reducing conditions consistent with magnetite + ilmenite rather than magnetite

+ hematite (Burt 1980; Černý 2002). Ready availability of Ti and Ca, the latter in excess over that needed for allanite-(Ce) and amphibole, could be critical for stabilization of makarochkinite in addition to, or instead of, gadolinite and danalite.

Høgtuvaite is a metamorphic mineral that crystallized under amphibolite facies conditions in quartzofeldspathic orthogneiss enriched in Be and other rare metals prior to metamorphism (Lindahl and Grauch 1988; Grauch et al. 1994). Although the average analysis of the mineralized orthogneiss (including høgtuvaite-bearing units) is slightly peraluminous [Al/(K + Na + 2Ca) = 1.04], the suite of minerals associated with høgtuvaite lacks Al-rich phases and is remarkably similar to that of the Pit 400 pegmatite (Appendix 1, Table 1). Notable differences are that phenakite is coeval with høgtuvaite and that ilmenite as independent grains and ferrocolumbite are absent at Høgtuva. The presence of Fe^{2+}-dominant Ti-Nb-Ta oxides suggests that both Fe^{2+} and Ti were more available in the Pit 400 pegmatite than in the Høgtuva gneiss for incorporation in the makarochkinite-høgtuvaite solid-solution.

MAKAROCHKINITE

Physical and optical properties

Makarochkinite forms equant masses 5–50 mm across; a few grains show 1 or 2 uneven faces (Polyakov et al. 1986). It is black in hand specimen; the streak is greenish black; the luster is vitreous; fluorescence was not observed. In hand specimen and thin sections of standard thickness, it is opaque, whereas in thin slivers (<1 μm), it transmits some light (see below). It is brittle and has a Moh's hardness of 5.5–6. Polyakov et al. (1986) reported imperfect "{110} and {110}" (sic) cleavages (given as {110} and $\{\bar{1}01\}$ in Bokiy et al. 1996), but we found no discernable cleavage in any of our samples; indeed, absence of cleavage was one of the features used to distinguish makarochkinite from amphibole in the field. Polyakov et al. (1986) reported the fracture as conchoidal, whereas the fracture is better characterized as uneven in our samples. Polyakov et al. (1986 and unpublished data) reported 3.87(1) g/cm^3 for the measured density (Westphal's balance). Our study of the neotype specimen (no. 400Shch-6), in which we used a micropycnometer and bromoform, gave 3.93(1) g/cm^3. The calculated densities are 3.88 g/cm^3 (Polyakov et al. 1986), 3.92 g/cm^3 (Yakubovich et al. 1990), and 3.933 g/cm^3 for the neotype specimen (Table 2).

Polyakov at al. (1986 and unpublished data) reported that makarochkinite is biaxial (sign not known) with $\alpha = 1.799 \pm 0.005$ and $\gamma = 1.86 \pm 0.01$ using high-index refractive liquids. Using the Fresnel equation, reflectance values (Appendix 2) obtained at 589 nm from the neotype specimen (400Shch-6) gave $\alpha = 1.835 \pm 0.014$ and $\gamma = 1.865 \pm 0.015$. $2V$, orientation, and dispersion are not known. Pleochroism is marked, but visible only in very thin slices: X = greenish brown, Y = yellowish brown, Z = reddish brown; $Y \leq X < Z$.

Chemical composition and compatibility index

Three specimens of makarochkinite in carbon-coated thin sections were analyzed (Table 2): no. 3319 from P. M. Kartashov, no. 89351 (type) from the Fersman Museum (courtesy of D.I. Belakovskiy), and no. 400Shch-6 (neotype), as well as høgtuvaite in a sample R. Grauch collected from the same outcrop as the type høgtuvaite sample (here designated as N86, the prefix used by Grauch et al. 1994, for specimens from this outcrop). An ARL-SEMQ electron microprobe was used to analyze elements with $Z > 10$ in three of the four samples; a Cameca SX100 electron microprobe was used for the neotype specimen (Table 2). Analytical conditions for the ARL were 15 kV accelerating voltage, 10 nA beam current, and a 3 μm spot size. Standards were kyanite (Si$K\alpha$), apatite (P$K\alpha$), $LiNbO_3$ (Nb$L\alpha$), $LiTaO_3$ (Ta$M\alpha$), rutile (Ti$K\alpha$), SnO_2 (Sn$L\alpha$), kyanite (Al$K\alpha$), hematite (Fe$K\alpha$), spessartine (Mn$K\alpha$), diopside (Mg$K\alpha$), diopside (Ca$K\alpha$), jadeite (Na$K\alpha$), orthoclase (K$K\alpha$), and $Y_2Al_5O_{12}$ (Y$L\alpha$), and the data were processed with a $\phi(\rho z)$ scheme in which the effect of BeO was included. Analytical conditions for the Cameca SX 100 were 15 kV accelerating voltage, 10 nA beam current, and 10 μm spot size; the data were processed using the X-Phi correction of Merlet (1994). The standards used for the neotype specimen were fayalite (Si$K\alpha$), $LiNbO_3$ (Nb$L\alpha$), $LiTaO_3$ (Ta$L\alpha$), rutile (Ti$K\alpha$), kyanite (Al$K\alpha$), magnetite (Fe$K\alpha$), rhodonite (Mn$K\alpha$), periclase (Mg$K\alpha$), wollastonite (Ca$K\alpha$), and jadeite (Na$K\alpha$). Constituents to be analyzed were selected on the basis of wavelength-dispersive scans, which indicated that Y and Sn contents were close to the limits of detection in the neotype specimen. The Fe^{2+}/Fe^{3+} ratio in makarochkinite was either measured using Mössbauer spectroscopy (see below) or calculated from stoichiometry assuming 14 cations and 20 oxygen atoms.

The Be content of no. 3319, no. 400Shch-6, and N86 was determined by refining Be vs. Si occupancies of the T1 and T4 sites without constraining the total Be content (the only constraint being 100% site occupancy and equal U_{eq} parameters); minor Be at the T2 site in høgtuvaite was revealed by consideration of the U_{eq} parameters. The Be contents were corrected for B, which cannot be distinguished from Be in the structure refinement. Estimated standard deviations (e.s.d.) range from 0.8–1.0% of the refined Be occupancies in makarochkinite to 1.2% in høgtuvaite, so precision of the Be contents could be roughly ± 1% relative or ± 0.03 wt% BeO.

Be, Li, and B were measured with a Cameca ims 4f ion microprobe at the University of New Mexico (UNM) using secondary-ion mass spectrometry (SIMS) and the approach of Grew et al. (2001). Be standards used in other studies, e.g., Be-doped synthetic granitic glasses (Evensen and London 2002) or surinamite (Grew et al. 2000, 2001), are not appropriate for makarochkinite; sample no. 3319 was used instead. Be measurements were made at a mass resolution of ~320 (routine conditions) and at ~1000, and comparison of the data sets confirmed that the lower resolution is adequate for makarochkinite. Repeated measurements of different grains or spots on a single grain of each sample during 3 or 4 SIMS sessions gave a reproducibility of ±2.3–3.7% relative or ± 0.06–0.1 wt% BeO. The resulting Be contents correlate well with Be contents determined independently by refinement of the T site occupancies (Table 2). Standards for Li and B included one or all three of the tourmaline standards analyzed by Dyar et al. (2001), as well as one or two prismatine standards (no. 112233 and no. BM1940,39) analyzed by Cooper (1997) and Cooper et al. (in preparation). Repeated measurements of Li and B from different grains or spots on a single grain of each sample gave a reproducibility of ±1–12% (26% for B in no. 3319) of the

TABLE 2. Composition of makarochkinite and høgtuvaite

	makarochkinite					høgtuvaite			
Sample		3319	3319	89351 (type)	400Shch-6 (neotype)	N86		N86-1A	N86-6B
Probe		ARL	ARL	ARL	Cameca	ARL			
Source	1	2	2	2	2	2	3*	3	3
					wt%				
SiO_2	30.09	31.34	31.12	31.12	30.94	31.67	31.60	31.57	32.15
P_2O_5	–	b.d.	–	–	–	b.d.	b.d.	b.d.	b.d.
Nb_2O_5	b.d.	0.85	0.93	0.81	0.58	0.15	0.159†	0.159†	–
Ta_2O_5	–	0.19	0.26	0.16	0.19	b.d.	–	–	–
TiO_2	6.02	4.65	4.95	5.87	5.60	2.19	2.77	2.28	4.17
SnO_2	–	0.03	0.27	0.27	b.d.	0.46	0.53	0.50	0.16
Al_2O_3	3.55	2.78	2.88	3.04	3.19	2.44	2.64	2.75	0.93
Σ FeO	36.92	41.81	41.39	40.52	42.06	46.12	45.18	45.48	44.71
Fe_2O_3	11.12	16.26‡	16.10‡	10.75§	14.02‡	20.50‡	19.03	20.02	18.81§
FeO	26.91	27.18‡	26.91‡	30.85§	29.45‡	27.67‡	28.06	27.47	27.78§
MnO	1.26	1.25	1.21	1.21	1.10	0.40	0.27	0.29	0.52
MgO	2.74	1.25	1.17	1.24	1.15	0.39	0.42	0.50	0.29
CaO	13.38	10.82	11.34	10.86	10.59	10.58	10.44	10.97	10.16
Na_2O	1.35	0.87	0.68	0.87	0.91	1.28	1.52	1.31	1.78
K_2O	0.30	b.d.	–	–	–	b.d.	b.d	b.d	b.d
BeO	2.32	2.85‖	2.85‖	–	2.62‖	3.11‖	2.65†	2.83†	3.00#
BeO**	–	–	–	2.70**	2.60**	2.98**	–	–	–
B_2O_3	–	0.055#	0.054**	0.018**	0.013**	0.019**	0.031†	0.031†	–
Y_2O_3	–	–	b.d.	0.17	b.d.	–	0.159†	0.159†	–
Li_2O	–	0.006#	0.006**	0.005**	0.005**	0.012**	0.011†	0.011†	–
ZnO	–	–	–	–	–	–	0.071†	0.071†	–
Sum	99.68††	100.37	100.73	99.94	100.35	100.86	100.36	100.92	99.76
Formulae (based on 20 oxygen atoms per formula unit)									
Si	4.395	4.505	4.462	4.522	4.472	4.563	4.588	4.553	4.676
Nb	0.000	0.055	0.060	0.053	0.038	0.010	0.010	0.010	0.000
Ta	–	0.007	0.010	0.006	0.007	0.000	–	–	–
Ti	0.661	0.502	0.534	0.641	0.609	0.237	0.303	0.247	0.456
Sn	–	0.002	0.015	0.016	0.000	0.027	0.031	0.029	0.009
Al	0.611	0.470	0.487	0.521	0.543	0.415	0.452	0.467	0.159
Fe^{3+}	1.222	1.759	1.737	1.175	1.525	2.223	2.079	2.173	2.059
Fe^{2+}	3.287	3.267	3.227	3.748	3.559	3.335	3.407	3.313	3.379
Mn	0.156	0.152	0.147	0.148	0.135	0.048	0.033	0.035	0.064
Mg	0.597	0.268	0.250	0.270	0.248	0.084	0.091	0.108	0.063
Ca	2.094	1.667	1.742	1.690	1.640	1.633	1.624	1.695	1.583
Na	0.382	0.242	0.190	0.246	0.254	0.357	0.428	0.366	0.502
Be	0.814	0.984	0.982	0.943	0.910	1.076	0.924	0.980	1.048
B	–	0.014	0.013	0.005	0.003	0.005	0.008	0.008	—
Y	–	–	0.000	0.013	0.000	–	0.012	0.012	—
Li	–	0.004	0.004	0.003	0.003	0.007	0.006	0.006	—
Zn	–	–	–	–	–	–	0.008	0.008	—
Sum	14.219	13.898	13.861	14.000	13.945	14.019	14.005	14.012	14.000

Notes: b.d. = below detection. Sums do not include Σ FeO or SIMS BeO when SREF BeO available. Sources of data: 1 = Polyakov et al. (1986); 2 = this paper using an ARL SEMQ or a Cameca SX 100 electron microprobe; 3 = Grauch et al. (1994).

* Preferred composition.

† ICP-AES data for sample N86-1.

‡ Fe^{3+}/Fe^{2+} ratio from Mössbauer spectroscopy.

§ Fe^{3+}/Fe^{2+} ratio calculated assuming 14 cations, 20 O.

‖ Refinement of Be occupancies of T1 and T4 sites and minor Be at the T2 site in høgtuvaite; B content deducted.

Assumed.

** Secondary ion mass spectroscopy (SIMS) using 3319 as a standard for Be.

†† Sum includes H_2O^- 0.07, H_2O^+ 0.35, LOI 0.22.

measured value, i.e., 0.4–7 ppm for < 100 ppm Li or B (168 ± 44 ppm B in no. 3319).

The Gladstone-Dale relation (Mandarino 1981) gave a compatibility index for sample 400Shch-6 of 0.020 (excellent) and 0.044 (good), using the refractive indices $(\alpha + \gamma)/2$ based on reflectance spectra and high-index refractive liquids, respectively.

CRYSTALLOGRAPHIC PROPERTIES OF MAKAROCHKINITE AND HØGTUVAITE

Powder X-ray diffraction of makarochkinite

Powder X-ray diffraction data for three different samples, together with the calculated cell volume for no. 3319, are compiled in Appendix 3. The powder pattern agrees well with that calculated from the crystal structure of sample no. 3319.

Single-crystal X-ray diffraction of makarochkinite and høgtuvaite

Black platy fragments of makarochkinite no. 3319 (0.19 × 0.13 × 0.07 mm), no. 400Shch-6 (0.21 × 0.14 × 0.04 mm), and høgtuvaite N86 (0.25 × 0.12 × 0.03 mm) were selected for single-crystal study. The crystals were mounted on a Bruker-AXS diffractometer equipped with a Mo$K\alpha$ rotating-anode generator and a SMART 1K area detector. The raw intensity data were processed with the SAINT software (Bruker 2000) and corrected for absorption with the SADABS program (Sheldrick 1996). The structure refinements were done with the SHELXL97 program

TABLE 3. Details of the single-crystal X-ray refinements

Mineral	Makarochkinite*	Makarochkinite*	Høgtuvaite*
Sample number	3319	400Shch-6	N86
Space group	$P\bar{1}$	$P\bar{1}$	$P\bar{1}$
a (Å)	10.373(2)	10.355(2)	10.322(1)
b (Å)	10.768(3)	10.751(3)	10.729(1)
c (Å)	8.878(1)	8.873(2)	8.8624(8)
α (°)	105.794(10)	105.707(8)	105.802(2)
β (°)	96.183(8)	96.227(6)	96.185(2)
γ (°)	124.934(6)	124.861(6)	124.758(1)
V (Å)^3	737.4(2)	735.7(3)	731.7(1)
Z	2	2	2
Calc. density (g/cm^3)	3.929	3.948	3.966
μ (mm^{-1}) (Mo$K\alpha$)	6.448	6.551	6.715
2θ max (°)	72.48	72.58	54.98
h_{min}, h_{max}	–17, 15	–16, 16	–13, 13
k_{min}, k_{max}	–17, 17	–16, 17	–13, 13
l_{min}, l_{max}	–14, 14	–14, 11	–11, 11
Unique reflections	6788	6497	6776 †
Absorption correction		SADABS program	
T_{min}/T_{max}	0.475	0.617	0.748 (twin 1), 0.747 (twin 2)†
R_{int}	0.057	0.059	n/a
Parameters refined	311	311	313
Twinning parameter	n/a	n/a	0.293(3)†
Reflections used	6788	6497	6776
Reflections [$I > 2\sigma(I)$]	4740	4142	4996
Weighting scheme		$w = 1 / [\sigma^2(F_o^2) + (A.P)^2]$ $P = (F_o^2 + 2F_c^2) / 3$	
Weighting parameter A	0.041	0.0374	0.0577
Extinction coeff.	0.0130(6)	0.0189(6)	n/a
R(F) [$I > 2\sigma(I)$]	0.041	0.049	0.043
$wR(F^2)$ (all)	0.0896	0.096	0.126
$\Delta\rho_{min}$ (e. Å^{-3})	–2.01	–1.17	–1.18
$\Delta\rho_{max}$ (e. Å^{-3})	1.87	1.36	0.84

*Simplified chemical formulae based on 14 cations per 20 oxygen atoms: no. 3319 = $(Ca_{1.76}Na_{0.20}Mn_{0.04})(Fe_{5.07}Ti_{0.54}Mg_{0.25}Nb_{0.07}Al_{0.05}Sn_{0.02})(Si_{4.51}Be_{1.00}Al_{0.44}Fe_{0.05})O_{20}$; no. 400Shch-6 = $(Ca_{1.69}Na_{0.21}Mn_{0.10})(Fe_{5.11}Ti_{0.59}Mg_{0.25}Nb_{0.04}Ta_{0.01})(Si_{4.49}Be_{0.90}Al_{0.54}Fe_{0.07})O_{20}$ and N86 = $(Ca_{1.70}Na_{0.30})(Fe_{5.58}Ti_{0.24}Mg_{0.12}Al_{0.03}Sn_{0.03})(Si_{4.56}Be_{1.06}Al_{0.35}Fe_{0.03})O_{20}$. Calculated densities based on these formulae (cf. text).
† The høgtuvaite crystal contained two twin components related by a two-fold rotation around the [12$\bar{2}$] direction of the triclinic unit cell (see text). The pseudomerohedral twinning leads to the presence of extra reflections.

(Sheldrick 1997). Details of the data collection and refinement are summarized in Table 3.

Structure refinement of makarochkinite. The selected crystals for no. 3319 and no. 400Shch-6 were untwinned, with triclinic unit-cells typical of the aenigmatite group (Table 3). The absence of twinning (Barbier et al. 2001) is consistent with the finding reported by Yakubovich et al. (1990). The refinements were done on the basis of simplified chemical compositions derived from the refinement of Be occupancies (see below) and the electron and ion microprobe analyses, viz., $^{[VII]}(Ca_{1.76}Na_{0.20}Mn_{0.04})$ $^{[VI]}(Fe_{5.07}Ti_{0.54}Mg_{0.25}Nb_{0.07}Al_{0.05}Sn_{0.02})$ $^{[IV]}(Si_{4.51}Be_{1.00}Al_{0.44}Fe_{0.05})O_{20}$ and $^{[VII]}(Ca_{1.69}Na_{0.21}Mn_{0.10})$ $^{[VI]}(Fe_{5.11}Ti_{0.59}Mg_{0.25}Nb_{0.04}Ta_{0.01})$ $^{[IV]}(Si_{4.49}Be_{0.90}Al_{0.54}Fe_{0.07})O_{20}$ for no. 3319 and no. 400Shch-6, respectively. The tetrahedral Be occupancies (Table 4) quickly converged to values near 50% at T1 and T4 (with e.s.d. values of 0.5%), in agreement with the previous structure determination by Yakubovich et al. (1990). The average <T-O> bond lengths and the U_{eq} parameters indicated that Al should be located at T3 with minor Fe^{3+}. Some minor redistribution of Al may well occur at the T2, T5, and T6 sites but it was not investigated further. Examination of the M-O distances and U_{eq} parameters led to the assignment of all Ti^{4+} to M7. The longer <M-O> distances for the M1-6 sites are consistent with mixed Fe/Mg, occupancies, which were refined by using the total Mg content as a constraint (with e.s.d. values of 0.2–0.3%). Due to the overall Ti content of makarochkinite, Ti is the dominant species at M7, followed by Fe and minor high-valence cations, viz., (54% Ti + 32% Fe + 7% Nb + 5% Al + 2% Sn) in no. 3319 and (59% Ti + 37% Fe + 4% Nb + 1% Ta) in no. 400Shch-6. As a check, the Ti/Fe content of M7 in no. 400Shch-6 was further refined and the result (66% Ti + 29% Fe, with 4% Nb + 1% Ta) was consistent with the assignment of all Ti to the M7 site.

TABLE 4. Site occupancies* and average bond lengths (Å) in makarochkinite and høgtuvaite (italics)

	%Fe	%Mg	%Ti	<M-O>
M1 (no. 3319)	89	11	–	2.073
M1 (no. 400Shch-6)	90	10	–	2.075
M1	*96*	*4*	–	*2.058*
M2 (no. 3319)	96	4	–	2.088
M2 (no. 400Shch-6)	98	2	–	2.092
M2	*98*	*2*	–	*2.069*
M3 (no. 3319)	96	4	–	2.114
M3 (no. 400Shch-6)	97	3	–	2.115
M3	*100*	–	–	*2.107*
M4 (no. 3319)	92	8	–	2.125
M4 (no. 400Shch-6)	94	6	–	2.123
M4	*97*	*3*	–	*2.109*
M5 (no. 3319)	95	5	–	2.109
M5 (no. 400Shch-6)	91	9	–	2.102
M5	*94*	*6*	–	*2.112*
M6 (no. 3319)	98	2	–	2.139
M6 (no. 400Shch-6)	99	1	–	2.139
M6	*100*	–	–	*2.132*
M7† (no. 3319)	32	–	54	2.036
M7‡ (no. 400Shch-6)	37	–	59	2.031
M7§	*70*	–	*24*	*2.039*
	%Ca	%Na	%Mn	<M-O>
M8 (no. 3319)	89	11	–	2.448
M8 (no. 400Shch-6)	79	16	5	2.445
M8	*73*	*27*	–	*2.445*
M9 (no. 3319)	88	8	4	2.459
M9 (no. 400Shch-6)	90	5	5	2.526
M9	*98*	*2*	–	*2.520*
	%Si	%Be	%Al	<T-O>
T1 (no. 3319)	52	48	–	1.646
T1 (no. 400Shch-6)	56	44	–	1.648
T1	*50*	*50*	–	*1.644*
T2 (no. 3319)	100	–	–	1.650
T2 (no. 400Shch-6)	100	–	–	1.648
T2	*90*	*5*	*5*	*1.643*
T3‖ (no. 3319)	52	–	43	1.690
T3# (no. 400Shch-6)	39	–	54	1.685
*T3***	*67*	–	*30*	*1.687*
T4 (no. 3319)	48	52	–	1.633
T4 (no. 400Shch-6)	54	46	–	1.633
T4	*49*	*51*	–	*1.632*
T5 (no. 3319)	100	–	–	1.648
T5 (no. 400Shch-6)	100	–	–	1.643
T5	*100*	–	–	*1.641*
T6 (no. 3319)	100	–	–	1.646
T6 (no. 400Shch-6)	100	–	–	1.645
T6	*100*	–	–	*1.643*

* e.s.d. values on occupancies are 0.3% (M1-6), 0.3% (M8, M9), 0.5% (T1, T4) for makarochkinite and 0.3% (M1-6), 0.4% (M8, M9), and 0.6% (T1,T4) for høgtuvaite.
† M7 also contains 7% Nb, 5% Al, and 2% Sn.
‡ M7 also contains 4% Nb and 1% Ta.
§ M7 also contains 3% Sn and 3% Al.
‖ T3 also contains 5% Fe.
T3 also contains 7% Fe.
** T3 also contains 3% Fe.

Structure refinement of høgtuvaite. As expected from the original study reporting pervasive polysynthetic twinning in høgtuvaite (Grauch et al. 1994), the crystal fragment of N86 used in the present study was found to be twinned. The diffraction pattern was initially indexed on a large monoclinic unit-cell

(a = 10.325, b = 29.58, and c = 10.130 Å, β = 108.74°) similar to that observed for other twinned minerals of the aenigmatite group, such as krinovite (Merlino 1972; Bonaccorsi et al. 1989), sapphirine-1*A* (Merlino 1980), rhönite (Bonaccorsi et al. 1990), and the krinovite analogue, $Na_2(Mg,Fe)_6(Ge,Fe)_6O_{20}$ (Barbier 1995a). The true triclinic unit-cell of høgtuvaite (Table 3) was derived from the large monoclinic cell by the transformation matrix (0 0 –1; 1/2 1/4 3/4; 1/2 –1/4 1/4). The refinement of site occupancies (Table 4) was based on a simplified chemical composition derived from electron microprobe analysis of høgtuvaite N86, viz., $^{[VII]}(Ca_{1.65}Na_{0.35})\,^{[VI]}(Fe_{5.60}Ti_{0.24}Mg_{0.08}Al_{0.03}Sn_{0.03})\,^{[IV]}(Si_{4.56}Be_{1.06}Al_{0.35}Fe_{0.03}O_{18})O_2$. The Be content of høgtuvaite is slightly larger than for makarochkinite and the refinement indicated the presence of minor Be at T2 (as determined from refinement of the U_{eq} parameter) besides the 50% Be occupancies at T1 and T4. The shortest M-O distances were again found for M7 which led to the assignment of all Ti, with Fe and minor Sn and Al, to this site. Due to the lower Ti content of høgtuvaite, however, the M7 site is still predominantly occupied by Fe (70% Fe, 24% Ti, 3% Sn, 3% Al). This cation population is consistent with the slightly longer <M7-O> average bond length observed in høgtuvaite (2.039 Å) vs. makarochkinite (2.031 Å).

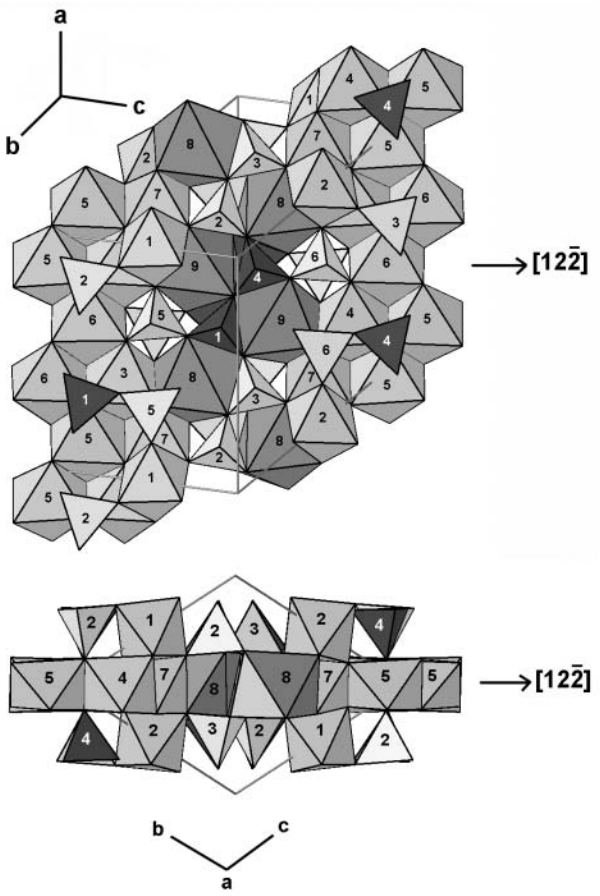

FIGURE 2. View of the makarochkinite structure approximately along the [233] (top) and [100] (bottom) directions. The [12$\bar{2}$] direction in the plane of the figure corresponds to a pseudo twofold axis. The same labeling scheme is used for the cation sites of makarochkinite and høgtuvaite.

The final agreement indices for the makarochkinite and høgtuvaite refinements are given in Table 3; selected bond lengths, selected tetrahedral chain bond angles, and the anisotropic displacement parameters in Appendix 4. Probably as a result of using a twinned data set, the e.s.d. values for the atom coordinates, site occupancies, and displacement parameters are slightly larger for høgtuvaite than for makarochkinite.

Comparison of the makarochkinite and høgtuvaite structures

The geometries of both structures are very similar and only the makarochkinite structure is shown in Figure 2. The main structural features have been described previously for other minerals of the aenigmatite group (e.g., Bonaccorsi et al. 1990), and the emphasis here is on the cation distributions.

The M8 and M9 sites are seven-coordinated, not counting one longer M-O bond of approximately 3 Å for each site. The edge sharing occurring between these polyhedra and the tetrahedra (Fig. 2) accounts for the higher Ca-content at M9 (sharing edges with Be-rich T1 and T4), and the preference of Na for M8 (sharing an edge with Al-rich T3). Similar Ca/Na distributions have been observed in another makarochkinite sample (Yakubovich et al. 1990) and in serendibite (Van Derveer et al. 1993), and are consistent with bond-valence calculations around the O atoms and the minimization of cation-cation repulsion across the shared edges.

The distribution of tetrahedral Be in makarochkinite and høgtuvaite corresponds to a concentration at the most polymerized T1 and T4 tetrahedra, each sharing corners with three other tetrahedra (Fig. 2). In both makarochkinite and høgtuvaite, the Be content at T1 and T4 averages 45 to 50%, which accommodates all the Be present in makarochkinite (0.9–1.0 Be per formula unit). This distribution is similar to that observed in other Be-bearing minerals, such as khmaralite (Barbier et al. 1999) and surinamite (Barbier et al. 2002), and in synthetic beryllian sapphirine (Christy et al. 2002). The limiting 50% Be occupancy at T1 and T4 avoids the strong underbonding of the bridging O atom that would occur if both sites were simultaneously occupied by Be (Christy et al. 2002). In høgtuvaite, the total Be content exceeds 1 atom per formula unit and the "excess" Be is accommodated at T2 (Table 4), a site corresponding to T4 in khmaralite,

TABLE 5. Cation occupancy of the M7 octahedral site in structures of the aenigmatite group

Mineral	M7 occupancy (%)	Reference
høgtuvaite	70 Fe + 24 Ti + 3 Sn + 3 Al	N86, this work
makarochkinite	59 Ti + 37 Fe + 4 Nb + 1 Ta	400Shch-6, this work
makarochkinite	54 Ti + 32 Fe + 7 Nb + 5 Al + 2 Sn	3319, this work
makarochkinite	50 Ti + 50 Fe	Yakubovich et al. (1990)
rhönite (Scharnhausen)	100 Ti	Bonaccorsi et al. (1990)*
rhönite (Allende)	56 Mg + 44 Ti	Bonaccorsi et al. (1990)*
krinovite	100 Cr	Bonaccorsi et al. (1989)
Fe-Ge krinovite analogue	100 Fe	Barbier (1995a)
aenigmatite	59 Ti + 41 Fe	Cannillo et al. (1971)
serendibite (Johnsburg)	100 Al	Van Derveer et al. (1993)

*The rhönite refinements show rather large variations for the U_{eq} parameters of the M1-7 sites that cast doubt on the exact cation distributions.

which is occupied by 3% Be (Barbier et al. 1999).

The major distinction between makarochkinite and høgtuvaite arises from the Ti content and the occupancy of the M7 octahedral site. In all structures of the aenigmatite group, the M7 octahedron shares the most (seven) edges with adjacent polyhedra and accommodates the most highly charged cations, such as Al^{3+}, Fe^{3+}, Cr^{3+}, Ti^{4+}, and Nb^{5+} (Table 5). This cation ordering is similar to the complete ordering of octahedral Si^{4+} in the high-pressure anhydrous phase B ($Mg_{14}Si_5O_{24}$; Finger et al. 1991), octahedral As^{5+}, in aerugite ($Ni_{8.5}As_3O_{16}$; Fleet and Barbier 1989), and octahedral Ge^{4+} in the related germanate $Co_{10}Ge_3O_{16}$ (Barbier 1995b). In these structures, the small and highly charged Si^{4+}, As^{5+} and Ge^{4+} cations fully occupy the octahedron with the most shared edges (twelve) in rock salt type clusters. This particular ordering of highly charged cations can be seen as the result of a synergy between the distribution of electrostatic potential in the crystal structure and the reduction in octahedral volume, both associated with the pattern and number of shared edges for a given octahedron. In both makarochkinite and høgtuvaite, the relatively minor Ti contents (0.59 and 0.24 Ti per formula unit, respectively) are entirely accommodated at the M7 site and Ti is the dominant M7 species in makarochkinite.

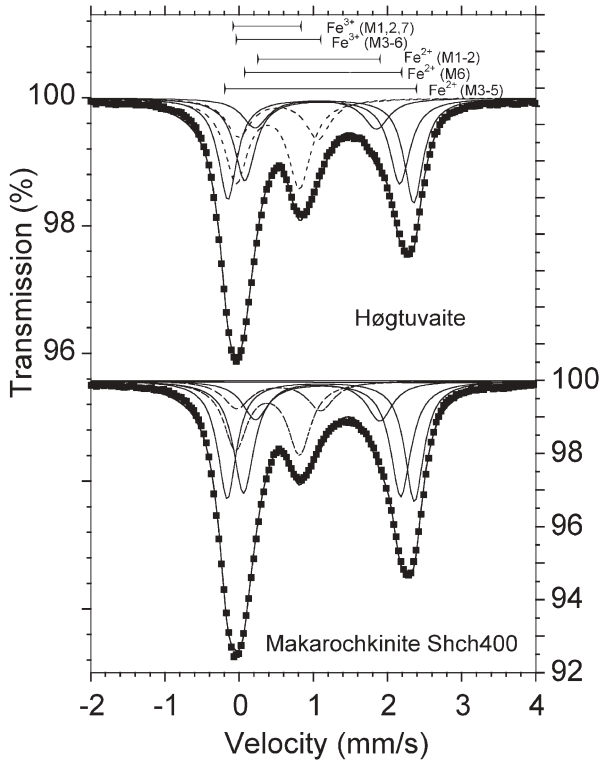

FIGURE 3. Fitted Mössbauer spectra of makarochkinite 400Shch-6 and høgtuvaite N86 at room temperature. Filled squares represent the recorded spectra. The solid line passing through the squares is the sum of the five fitted quadrupole doublets, which are shown as solid lines for Fe^{2+} and dashed lines for Fe^{3+}. Quadrupole splittings for the five doublets are shown as bars.

SPECTROSCOPY OF MAKAROCHKINITE AND HØGTUVAITE

Mössbauer spectroscopy

Absorbers for ^{57}Fe Mössbauer spectroscopy were prepared by pressing finely ground mineral concentrates with a powdered acrylic resin (transoptic powder) into self-supporting discs with an Fe thickness of ca. 2 mg/cm^2. Room-temperature spectra were recorded with a constant acceleration system as described in Barbier et al. (2002). The spectra were fitted using a least-square fitting program (Jernberg and Sundqvist 1983) assuming Lorentzian peak shapes and equal intensity and line width of the components of each quadrupole doublet. Although fitting of Voigt functions seemed reasonable, we found that application of this approach (Rancourt and Ping 1991) did not improve the spectral analysis.

The Mössbauer spectra of makarochkinite and høgtuvaite are characterized by three well-resolved absorption bands that show variable degree of asymmetry (Fig. 3). A model comprising five quadrupole doublets resulted in convergent fits (Table 6). Fewer doublets resulted in fits with distinctly higher χ^2 values, whereas more doublets did not significantly lower the value and did not always give convergent fits.

On the basis of the variations in mean M-O distances and degree of distortion from O_h symmetry, the seven Fe-bearing [VI]-coordinated sites in makarochkinite and høgtuvaite may be divided into three groups: (1) M1, M2, and M7 are characterized by comparatively short M-O distances and small to moderate distortion; (2) M3, M4, and M5, by longer M-O bonds and a high degree of distortion; and (3) M6 is also characterized by long M-O distances but the distortion from O_h symmetry is less. On the basis of the variations in M-O distances, it is anticipated that the Mössbauer centroid shift (CS) for quadrupole doublets due to both Fe^{2+} and Fe^{3+} should increase in the order (M1, M2, M7) < (M3, 4, 5) ≤ M6. The CS-values for doublets due to [VI]-coordinated Fe^{3+} in oxygen-based structures are in general

TABLE 6. Mössbauer hyperfine parameters and intensities at room temperature

	CS mm/s	DQ mm/s	*w* mm/s	*I* %
makarochkinite 3319 (χ^2 = 5.309)				
Fe^{2+} (M1-2)	1.04	1.64	0.38	10
Fe^{2+} (M3-5)	1.10	2.51	0.30	30
Fe^{2+} (M6)	1.12	2.11	0.33	25
Fe^{3+} (M1,2,7)	0.39	0.84	0.36	24
Fe^{3+} (M3-6)	0.53	1.08	0.42	11
makarochkinite 400Shch-6 (χ^2 = 9.824)				
Fe^{2+} (M1,2)	1.06	1.68	0.41	12
Fe^{2+} (M3-5)	1.10	2.52	0.30	29
Fe^{2+} (M6)	1.12	2.12	0.34	29
Fe^{3+} (M1,2,7)	0.39	0.87	0.37	22
Fe^{3+} (M3-6)	0.56	1.18	0.42	8
høgtuvaite N86 (χ^2 = 8.966)				
Fe^{2+} (M1,2)	1.04	1.67	0.41	11
Fe^{2+} (M3-5)	1.10	2.51	0.30	26
Fe^{2+} (M6)	1.13	2.10	0.31	23
Fe^{3+} (M1,2,7)	0.39	0.86	0.36	28
Fe^{3+} (M3-6)	0.53	1.09	0.38	12

Note: CS = centroid shift; DQ = quadrupole splitting; *w* = full width at half maximum; *I* = intensity. Estimated error of Mössbauer hyperfine parameters is 0.02

considerably smaller than for Fe^{2+} at similar sites and in similar substances. The relatively small distortions of the M1, M2, and M7 octahedral sites are likely to result in smaller quadrupole splittings as compared to doublets caused by Fe^{3+} at the remaining structural sites. Quadrupole splitting of Fe^{2+} doublets is not exclusively an effect of the geometry of the Fe-centered site and consequently predictions solely based on geometric relations are not fully reliable. However, as a first approximation it is reasonable to assume that a quadrupole doublet due to Fe^{2+} at the M6 site may be distinguished from Mössbauer absorption doublets caused by Fe^{2+} at the M3, M4, and M5 sites by a smaller quadrupole splitting. Tentative assignments of the fitted quadrupole doublets based on these structural considerations are presented together with the obtained hyperfine parameters of the fitted quadrupole doublets in Table 6.

Due to the strongly overlapping quadrupole doublets caused by ferrous and ferric iron at M3-M6, it is not possible to determine the ferrous/ferric ratios at each of these sites with reasonable accuracy. Likewise, it is not possible to obtain a detailed picture of the distribution of Fe^{3+} and Fe^{2+} at each of the remaining sites (M1, M2, and M7). However, Mössbauer intensity data strongly suggest that Fe^{3+}preferentially occupies the M1, M2, and M7 sites [$Fe^{3+}/(Fe^{2+} + Fe^{3+}) \approx 0.7$], whereas Fe^{2+} is dominant at the M3-M6 sites [$Fe^{3+}/(Fe^{2+} + Fe^{3+}) \approx 0.2$].

Optical absorption spectroscopy

Due to the almost opaque character of makarochkinite and høgtuvaite it was extremely difficult to produce suitable absorbers for optical spectroscopy, and we had no success with høgtuvaite. For makarochkinite, it was possible to obtain extremely thin crystal slivers with reasonably sized areas by crushing small crystal fragments between glass slides. Optical absorption spectra (Fig. 4) were obtained at room temperature from thin (≤1 μm) single-crystal fragments dispersed in immersion medium (glycerol). Optical orientation of the crystal fragments was aided by observation of optical interference figures under conoscopic illumination. The optical spectra were recorded with a Zeiss MPM800 single-beam spectrometer (e.g., Barbier et al. 2002) at a spectral resolution of 5 nm in the UV/VIS range and 10 nm in the NIR region. The measure spot was 15 μm and glycerol was used as a reference medium.

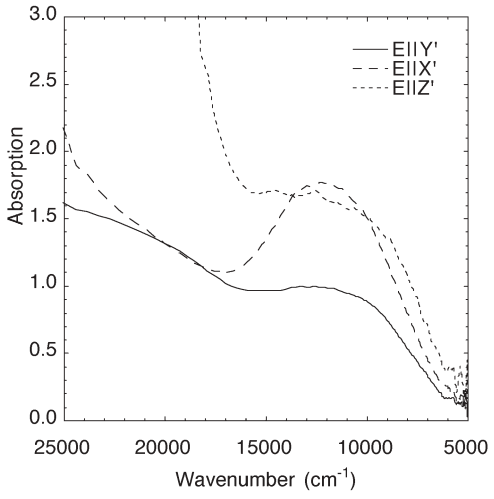

FIGURE 4. Polarized optical-absorption spectra of thin slivers of makarochkinite 400Shch-6.

The polarized optical-absorption spectra of makarochkinite are in all three principal directions dominated by a strong UV-absorption edge extending through the visible spectral region. In addition, all three spectra show an intense and very broad absorption band centered at ca 12000 cm^{-1} (Fig. 4). This absorption band is pleochroic: $X \approx Z > Y$. The band shows spectral features (large band width and high absorption coefficient) associated with intervalence charge transfer bands (Mattson and Rossman 1987). In view of the fact that Fe^{2+} ($3d^6$) and Fe^{3+} ($3d^5$) are present at very high concentrations in makarochkinite, it is reasonable to assign this band to Fe^{2+}-Fe^{3+} IVCT. For the present sample, which contains moderate amounts of Ti in addition to Fe, an alternative assignment would be Fe^{2+}-Ti^{4+} IVCT, but such bands are expected to occur at higher energy (e.g., Burns 1993). The energy of the IVCT band in the makarochkinite spectra is at the lower end recorded for Fe^{2+}-Fe^{3+} IVCT in the spectra of silicate minerals (e.g., Mattson and Rossman 1987), but comparable energies occur in spectra of densely packed Fe-rich silicate minerals such as ilvaite (Amthauer and Rossman 1984).

Due to the strong optical absorption of makarochkinite, it was not possible to fully characterize the optical properties, including determinations of the geometric relation between crystallographic and optical directions. Nonetheless, the pleochroism of the observed Fe^{2+}-Fe^{3+} IVCT-band provides some

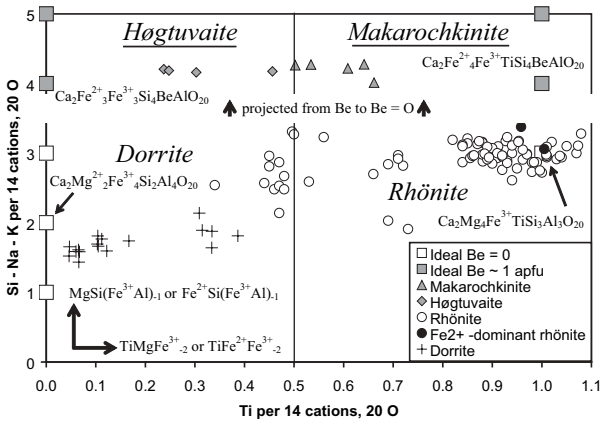

FIGURE 5. Natural and end-member compositions of terrestrial rhönite with less than 1.1 Ti per formula unit and related minerals projected along $CaAl(NaSi)_{-1}$ and $CaAl(KSi)_{-1}$ onto the alkali-free plane (modeled on Kunzmann, 1999, Fig. 7). The Be-bearing compositions, all with $Fe^{2+} > Mg$, and the Be-free compositions are related by the substitution $BeSiAl_{-2}$, which is indicated by the breaks in the lines bounding the plotted points, but the beryllian compositions have been projected from Be onto the plane for Be = 0. Names of minerals containing essential Be are underlined. Other minerals are $Mg > Fe^{2+}$ except for a few Fe^{2+}-dominant analogues of rhönite. Circles refer to minerals reported as rhönite by Boivin (1980); Bonaccorsi et al. (1990); Cameron et al. (1970); Grapes et al. (2003); Grünhagen and Seck (1972); Johnston and Stout (1984, 1985); Kunzmann (1989); Kyle and Price (1975); Magonthier and Velde (1976); Olsson (1984); and Prestvik et al. (1999). Included with dorrite (crosses) are the Fe^{3+}-rich "melilite" of Foit et al. (1987) and "mineral X_1" of Havette et al. (1982). Other sources of data: Cosca et al. (1988); Grauch et al. (1994); and this study.

constraints. The high intensity for the IVCT-band in **E**||*X*' and **E**||*Z*'-directions suggests that the optical *X*- and *Z*-directions must be located within a plane where the number of edge-sharing Fe^{3+} (M1/M2/M7)-Fe^{2+}(M3/M4/M5/M6) octahedral pairs are high and perpendicular to this plane (optical *Y*-direction) the structure must be depleted in such pair arrangements. One such plane $(1,\bar{1},0)$ is identical to the optic-axial plane in aenigmatite and rhönite, which suggests that the orientation of the optic plane is the same for makarochkinite and other aenigmatite-group minerals.

Makarochkinite as a distinct species in the aenigmatite-sapphirine-surinamite group

Makarochkinite is compositionally closest to rhönite and høgtuvaite; all are Ca-dominant members of the aenigmatite-sapphirine-surinamite group. Kunzmann (1989, 1999) proposed $Ca_2Mg_4Fe^{3+}TiAl_3Si_3O_{20}$ as the end-member formula for rhönite; this component is dominant in most rhönite, although a few are Fe^{2+}-dominant analogues and others have higher Al/Si ratios (Fig. 5). When høgtuvaite was first introduced as a new species with an end-member formula $Ca_2(Fe^{2+}_5Ti)O_2[Si_5Be]O_{18}$, it was hypothesized that the main distinction between høgtuvaite and rhönite was the 1 Be per formula unit, which was supposed to be sufficient to predominate at one tetrahedral site, although the crystal structure could not be refined to confirm this (Grauch et al. 1994; Burt 1994).

Our refinements of the crystal structures of høgtuvaite and makarochkinite show that Be is present at two or more tetrahedral sites, but never clearly dominant at either. Thus the distinction between høgtuvaite and makarochkinite on the one hand, and rhönite on the other, must still be argued on the basis of stoichiometry (~1 Be per formula unit) rather than on site occupancy, as well as by the dominance of Fe^{2+} over Mg at the M sites.

Høgtuvaite and makarochkinite are distinct from one another because Ti is the dominant cation at M7 in makarochkinite, whereas Fe^{3+} is the dominant cation at M7 in høgtuvaite (Table 5). Occupancy of M7 has been used as a criterion for distinguishing other species of the aenigmatite group. The best example is the distinction between wilkinsonite, $Na_2Fe^{2+}_4Fe^{3+}_2Si_6O_{20}$, and aenigmatite, $Na_2Fe^{2+}_5TiSi_6O_{20}$ (Duggan 1990). Cannillo et al. (1971) reported the cation population of M7 as 59(5)% Ti^{4+} and 41% Fe^{2+} in aenigmatite. In the absence of a structure refinement of wilkinsonite, Duggan (1990) presumed an analogy with aenigmatite and concluded that M7 would be dominated by Fe^{3+} in wilkinsonite. Kunzmann (1999, Figs. 4 and 6) showed the division between the two species at 0.5 Ti^{4+}, i.e., wilkinsonite-aenigmatite is analogous to høgtuvaite-makarochkinite as shown in Figure 5. In the case of dorrite, end-member $Ca_2Mg_2Fe^{3+}_4Al_4Si_2O_{20}$ (Cosca et al. 1988), and rhönite, end-member $Ca_2Mg_4Fe^{3+}TiAl_3Si_3O_{20}$, the situation is more complicated because several substitutions are involved. Kunzmann (1999, Figs. 4 and 7) showed one of the two divisions between the two minerals at 0.5 Ti^{4+} per formula unit.

Figure 5 suggests that the most appropriate end members are $Ca_2Fe^{2+}_3Fe^{3+}_3Si_4BeAlO_{20}$ for høgtuvaite and $Ca_2Fe^{2+}_4Fe^{3+}TiSi_4BeAlO_{20}$ for makarochkinite. The latter is one of the two compositions suggested by Hawthorne (2002) and Hawthorne and Huminicki (2002) as possible bona-fide end-members for makarochkinite. Makarochkinite end-member $Ca_2Fe^{2+}_4Fe^{3+}TiSi_4BeAlO_{20}$ is related to the Fe^{2+}-dominant rhönite end member $Ca_2Fe^{2+}_4Fe^{3+}TiSi_3Al_3O_{20}$ by a single substitution $BeSiAl_{-2}$, which is characteristic of several minerals incorporating Be (e.g., khmaralite-sapphirine; Christy et al. 2002), whereas relating høgtuvaite to a theoretical Fe^{2+}-dominant dorrite requires an additional substitution: $Fe^{3+}Al(Fe^{2+}Si)_{-1}$. Burt's (1994) end-member formula $Ca_2Fe^{2+}_5TiSi_5BeO_{20}$ is not appropriate for either makarochkinite or høgtuvaite because it ignores the substantial Fe^{3+} and Al contents in both minerals and because the Ti content did not exceed 0.5 Ti atoms per formula unit in any of the compositions reported by Grauch et al. (1994). In summary, makarochkinite is distinguished from høgtuvaite on the basis of Ti dominance at M7, the condition given by Hawthorne (2002) and Hawthorne and Huminicki (2002) as a prerequisite for recognizing makarochkinite as a valid species in the aenigmatite-sapphirine-surinamite group.

Acknowledgments

We thank N.I. Valizer and A.G. Bazhenov for their assistance in the field and continual consultation and T.M. Ryabukhina and E.D. Zenovich for X-ray diffractograms of minerals from Pit 400; D.I. Belakovskiy, Fersman Mineralogical Museum, and P.M. Kartashov for specimens of makarochkinite, and R. Grauch for specimens of høgtuvaite. A. Christy and F.C. Hawthorne are thanked for their insightful reviews. E.S.G.'s and M.G.Y.'s research was supported by U.S. National Science Foundation grants OPP-00887235 and MRI-0116235 to the University of Maine.

References cited

Amthauer, G. and Rossman, G.R. (1984) Mixed valence of iron in minerals with cation clusters. Physics and Chemistry of Minerals, 11, 37–51.

Baba, S., Grew, E.S., Shearer, C.K., and Sheraton, J.W. (2000) Surinamite: A high-temperature metamorphic beryllosilicate from Lewisian sapphirine-bearing kyanite-orthopyroxene-quartz-potassium feldspar gneiss at South Harris, N.W. Scotland. American Mineralogist, 85, 1474–1484.

Barbier, J. (1995a) Structure refinement of $Na_2(Mg,Fe)_6[(Ge,Fe)_6O_{18}]O_2$, a new aenigmatite-analog. Zeitschrift für Kristallographie, 210, 19–23.

——— (1995b) $Co_{10}Ge_3O_{16}$. Acta Crystallographica, C51, 343–345.

Barbier, J., Grew, E.S., Moore, P.B., and Su, S.-C. (1999) Khmaralite, a new beryllium-bearing mineral related to sapphirine: A superstructure resulting from partial ordering of Be, Al and Si on tetrahedral sites. American Mineralogist, 84, 1650–1660.

Barbier, J., Grew, E.S., Yates, M.G., and Shearer, C.K. (2001) Beryllium minerals related to aenigmatite. Geological Association of Canada and Mineralogical Association of Canada, Joint Annual Meeting, 26, 7.

Barbier, J., Grew, E.S., Hålenius, E., Hålenius, U., and Yates, M.G. (2002) The role of Fe and cation order in the crystal chemistry of surinamite, $(Mg,Fe^{2+})_3(Al,Fe^{3+})_3O[AlBeSi_3O_{15}]$: A crystal structure, Mössbauer spectroscopic, and optical spectroscopic study. American Mineralogist, 87, 501–513.

Boivin, P. (1980) Données expérimentales préliminaires sur la stabilité de la rhönite à 1 atmosphère. Application aux gisements naturels. Bulletin de Minéralogie, 103, 491–502.

Bokiy, G.B., Mozgova, N.N., and Sokolova, M.N., Eds. (1996) Minerals: Handbook. Vol IV, Part 3: Silicates. Additions to vol 3 and 4, 426 p. Nauka, Moscow.

Bonaccorsi, E., Merlino, S., and Pasero, M. (1989) The crystal structure of the meteoritic mineral krinovite, $NaMg_2CrSi_3O_{10}$. Zeitschrift für Kristallographie, 187, 133–138.

——— (1990) Rhönite: structural and microstructural features, crystal chemistry and polysomatic relationships. European Journal of Mineralogy, 2, 203–218.

Bruker (2000) SAINT program, version 6.02a. Bruker AXS Inc., Madison, Wisconsin.

Burns, R.G. (1993) Mineralogical Applications of Crystal Field Theory, ed. 2, 551 p. Cambridge University Press, Cambridge, U.K.

Burt, D.M. (1980) The stability of danalite, $Fe_4Be_3(SiO_4)_3S$. American Mineralogist, 65, 355–360.

——— (1994) Vector representation of some mineral compositions in the aenigmatite group, with special reference to høgtuvaite. Canadian Mineralogist, 32, 449–457.

Cameron, K.L., Carman, M.F., and Butler, J.C. (1970) Rhönite from Big Bend National Park, Texas. American Mineralogist, 55, 864–874.

Cannillo, E., Mazzi, F., Fang, J.H., Robinson, P.D., and Ohya Y (1971) The crystal structure of aenigmatite. American Mineralogist, 36, 427–446.

Černý, P. (1991) Fertile granites of Precambrian rare-element pegmatite fields: is geochemistry controlled by tectonic setting or source lithologies? Precambrian Research, 51, 429–468.

——— (1992) Geochemical and petrogenetic features of mineralization in rare-ele-

ment granitic pegmatites in the light of current research. Applied Geochemistry, 7, 393–416.
——— (2002) Mineralogy of beryllium in granitic pegmatites. In E.S. Grew, Ed., Beryllium: Mineralogy, Petrology and Geochemistry. Reviews in Mineralogy and Geochemistry, 50, 405–444. Mineralogical Society of America and the Geochemical Society, Washington, D.C.
Christy, A.G., Tabira, Y., Hölscher, A., Grew, E.S., and Schreyer, W. (2002) Synthesis of beryllian sapphirine in the system MgO-BeO-Al_2O_3-SiO_2-H_2O and comparison with naturally occurring beryllian sapphirine and khmaralite. Part 1: Experiments, TEM, and XRD. American Mineralogist, 87, 1104–1112.
Claflin, C.L. and Wise, M.A. (2000) Geochemistry of amphiboles in niobium-yttrium-fluorine-enriched pegmatites. Rocks and Minerals, 75, 172 and 174.
Cooper, M. (1997) The crystal chemistry of kornerupine, 199 p. M.Sc. Thesis, University of Manitoba, Winnipeg.
Cosca, M.A., Rouse, R.R., and Essene, E.J. (1988) Dorrite [$Ca_2(Mg_2Fe^{3+}_4)(Al_4Si_2)O_{20}$], a new member of the aenigmatite group from a pyrometamorphic melt-rock. American Mineralogist, 73, 1440–1448
Duggan, M.B. (1990) Wilkinsonite, $Na_2Fe^{2+}_4Fe^{3+}_2Si_6O_{20}$, a new member of the aenigmatite group from the Warrumbungle Volcano, New South Wales, Australia. American Mineralogist, 75, 694–701.
Dyar, M.D., Wiedenbeck, M., Robertson, D., Cross, L.R., Delaney, J.S., Ferguson, K., Francis, C.A., Grew, E.S., Guidotti, C.V., Hervig, R.L., Hughes, J.M., Husler, J., Leeman, W., McGuire, A.V., Rhede, D., Rothe, H., Paul, R.L., Richards, I., and Yates, M. (2001) Reference minerals for the microanalysis of light elements. Geostandards Newsletter, 25, 441–463
Evensen, J.M. and London, D. (2002) Experimental silicate mineral/melt partition coefficients for beryllium and the crustal Be from migmatite to pegmatite. Geochimica et Cosmochimica Acta, 66, 2239–2265.
Finger, L.W., Hazen, R.M., and Prewitt, C.T. (1991) Crystal structures of $Mg_{12}Si_4O_{19}(OH)_2$ (phase B) and $Mg_{14}Si_5O_{24}$ (phase AnhB). American Mineralogist, 76, 1–7.
Fleet, M.E. and Barbier, J. (1989) Structure of aerugite ($Ni_{8.5}As_3O_{16}$) and interrelated arsenate and germanate structural series. Acta Crystallographica, B45, 201–205.
Foit, F.F., Jr., Hooper, R.L., and Rosenberg, P.E. (1987) An unusual pyroxene, melilite, and iron oxide mineral assemblage in a coal-fire buchite from Buffalo, Wyoming. American Mineralogist, 72, 137–147.
Förster, H.-J. (1998) The chemical composition of REE-Y-Th-U-rich accessory minerals in peraluminous granites of the Erzgebirge-Fichtelgebirge region, Germany, Part I: The monazite-(Ce)-brabantite solid solution series. American Mineralogist, 83, 259–272.
Grapes, R.H., Wysoczanski, R.J., and Hoskin, P.W.O. (2003) Rhönite paragenesis in pyroxenite xenoliths, Mount Sidley volcano, Marie Byrd Land, West Antarctica. Mineralogical Magazine, 67, 639–651.
Grauch, R.I. and Lindahl, I. (1984) A unique suite of Sn- and Fe - Ti - Mn - Zn-oxides from Precambrain biotite gneisses, Nordland County, Norway. Geological Society of America Abstracts with Programs, 16, 523.
Grauch, R.I., Lindahl, I., Evans, H.T., Jr., Burt, D.M., Fitzpatrick, J.J., Foord, E.E., Graff, P.-R., and Hysingjord, J. (1994) Høgtuvaite, a new beryllian member of the aenigmatite group from Norway, with new X-ray data on aenigmatite. Canadian Mineralogist, 32, 439–448.
Grew, E.S., Yates, M.G., Barbier, J., Shearer, C.K., Sheraton, J.W., Shiraishi, K., and Motoyoshi, Y. (2000) Granulite-facies beryllium pegmatites in the Napier Complex in Khmara and Amundsen Bays, western Enderby Land, East Antarctica. Polar Geoscience, 13, 1–40.
Grew, E.S., Hålenius, U., Kritikos, M., and Shearer, C.K. (2001) New data on welshite, e.g., $Ca_2Mg_{3.8}Mn^{2+}_{0.6}Fe^{2+}_{0.1}Sb^{5+}_{1.5}O_2[Si_{2.8}Be_{1.7}Fe^{3+}_{0.65}Al_{0.7}As_{0.17}O_{18}]$, an aenigmatite-group mineral. Mineralogical Magazine, 65, 665–674.
Grünhagen, H. and Seck, H.A. (1972) Rhönit aus einem Melaphonolith vom Puy de Saint-Sandoux (Auvergne). Tschermaks Mineralogische und Petrographische Mitteilungen, 18, 17–38.
Hanson, S.L., Simmons, W.B., Falster, A.U., Foord, E.E., and Lichte, F.E. (1999) Proposed nomenclature for samarskite-group minerals: new data on ishikawaite and calciosamarskite. Mineralogical Magazine, 63, 27–36.
Havette, A., Clocchiatti, R., Nativel, P., and Montaggioni, L.F. (1982) Une paragenèse inhabituelle à fassaïte, mélilite et rhönite dans un basalte alcalin contaminé au contact d'un récif corallien (Saint-Leu, Ile de la Réunion). Bulletin de Minéralogie, 105, 364–375
Hawthorne, F.C. (2002) The use of end-member charge-arrangements in defining new mineral species and heterovalent substitutions in complex minerals. Canadian Mineralogist, 40, 699–710.
Hawthorne, F.C. and Huminicki, D.M.C. (2002) The crystal chemistry of beryllium. In E.S. Grew, Ed., Beryllium: Mineralogy, Petrology and Geochemistry. Reviews in Mineralogy and Geochemistry, 50, 333–403. Mineralogical Society of America and the Geochemical Society, Washington, D.C.
Jernberg, P. and Sundqvist, B. (1983) A versatile Mössbauer analysis program. Uppsala University, Institute of Physics (UUIP-1090).
Johnston, A.D. and Stout, J.H. (1984) A highly oxidized ferrian salite-, kennedyite-, forsterite-, and rhönite-bearing alkali gabbro from Kauai, Hawaii and its mantle xenoliths. American Mineralogist, 69, 57–68.
——— (1985) Compositional variation of naturally occurring rhoenite. American Mineralogist, 70, 1211–1216.
Kunzmann, T. (1989) Rhönit: Mineralchemie, Paragenese und Stabilität in alkalibasaltischen Vulkaniten (Ein Beitrag zur Minerogenese der Rhönit-Änigmatit-Mischkristallgruppe), 152 p. Ph.D. Dissertation, Ludwig-Maximilians-Universität, München.
——— (1999) The aenigmatite-rhönite mineral group. European Journal of Mineralogy, 11, 743–756.
Kyle, P.R. and Price, R.C. (1975) Occurrences of rhönite in alkalic lavas of the McMurdo Volcanic Group, Antarctica, and Dunedin Volcano, New Zealand. American Mineralogist, 60, 722–725.
Lindahl, I. and Grauch, R.I. (1988) Be-REE-U-Sn-mineralization in Precambrian granitic gneisses, Nordland County, Norway. In E. Zachrisson, Ed., Proceedings of the Seventh Quadrennial IAGOD Symposium, Luleå, Sweden, p. 583–594. E. Schweizerbart'sche Verlagsbuchhandlung, Stuttgart.
Magonthier, M.C. and Velde, D. (1976) Mineralogy and petrology of some Tertiary leucite – rhönite basanites from central France. Mineralogical Magazine, 40, 817–826.
Makarochkin, B.A. (1955) Ishkul'skiye excavations. Unpublished project report. In the archives of the Il'men Reserve.
——— (1978) Khlopinite from the Il'meny Mountains. In Popov, V.A. and Kornilov, Y.B. Eds., Investigations on the Mineralogy and Geochemistry of the Urals. Trudey Il'menskogo Gosudarstvennogo Zapovednika, 16, 82–83.
Mandarino, J.A. (1981) The Gladstone-Dale relationship: Part IV. The compatibility concept and its application. Canadian Mineralogist, 19, 441–450.
Mattson, S.M. and Rossman, G.R. (1987) Identifying characteristics of charge transfer transitions in minerals. Physics and Chemistry of Minerals, 14, 94–99.
Merlet, C. (1994) An accurate computer correction program for quantitative electron probe micro-analysis. Mikrochimica Acta, 114/115, 363–376.
Merlino, S. (1972) X-ray crystallography of krinovite. Zeitschrift für Kristallographie, 136, 81–88.
——— (1980) Crystal structure of sapphirine-1Tc. Zeitschrift für Kristallographie, 151, 91–100.
Olsson, H.B. (1984) Rhönite from Skåne (Scania), southern Sweden. Geologiska Föreningens i Stockholm Förhandlingar, 105, 281–286.
Polyakov, V.O., Cherepivskaya, G.Ye., and Shcherbakova, Ye.P. (1986) Makarochkinite — a new beryllosilicate. In New and little-studied minerals and mineral associations of the Urals. Akad Nauk SSSR Ural'skiy Nauchnyy Tsentr, Sverdlovsk, p. 108–110.
Popova, V.I., Popov, V.A., Polyakov, V.O., and Shcherbakova, Ye.P. (1996) Pegmatites of the Ilmen Mountains, ed. 2, 48 p. Rossiyskaya Akademiya Nauk, Ural'skoye Otdeleniye, Institut Mineralogii, Miass.
Prestvik, T., Torske, T., Sundvoll, B., and Karlsson, H. (1999) Petrology of early Tertiary nephelinites off mid-Norway. Additional evidence for an enriched endmember of the ancestral Iceland plume. Lithos, 46, 317–330
Rancourt, D.G. and Ping, J.Y. (1991) Voigt-based methods for arbitrary-shape static hyperfine parameter distributions in Mössbauer spectroscopy. Nuclear Instruments and Methods in Physics Research Section B, 58, 85–97.
Rasskazova, A.D. (1992) Geological structure of the Ilmen-Vishnevykh Mountains. In The Ufim Meridianal Structure of the Urals, p. 18-32. Rossiyskaya Akademiya Nauk, Ural'skoye Otdeleniye, Institut Mineralogii, Miass.
Shannon, R.D. (1976) Revised effective ionic radii and systematic studies of interatomic distances in halides and chalcogenides. Acta Crystallographica, A32, 751–767
Sheldrick, G.M. (1996) SADABS, Siemens area detector absorption correction software. University of Göttingen, Germany.
——— (1997) SHELXL97, program for the refinement of crystal structures. University of Göttingen, Germany.
Strunz, H. and Nickel, E.H. (2001) Strunz Mineralogical Tables. Chemical-Structural Mineral Classification System, ed. 9, 870 p. Schweizerbart'sche Verlagsbuchhandlung, Stuttgart.
Van Derveer, D.G., Swihart, G.H., Sen Gupta, P.K., and Grew, E.S. (1993) Cation occupancies in serendibite: A crystal structure study. American Mineralogist, 78, 195–203.
Warner, J.K. and Ewing, R. C. (1993) Crystal chemistry of samarskite. American Mineralogist, 78, 419–424.
Wise, M. (1999) Characterization and classification of NYF-type pegmatites. Canadian Mineralogist, 37, 802–803.
Yakubovich, O.V., Malinovskii, Yu. A., and Polyakov, V.O. (1990) Crystal structure of makarochkinite. Kristallografiya, 35, 1388–1394. [English translation: Soviet Physics and Crystallography, 35, 818–822].

MANUSCRIPT RECEIVED JULY 2, 2004
MANUSCRIPT ACCEPTED DECEMBER 26, 2004
MANUSCRIPT HANDLED BY BRENT OWENS